Geology, Geophysics & Environment 2025, vol. 51 (3): 301–316

Rare earth elements in supergene zone: a case study of the xenotime-(Y)-chernovite-(Y) solid solution from Rędziny, Sudetes, SW Poland

Bożena Gołębiowska[1], Natalia Chmaj[2], Adam Włodek[3], Monika A. Kusiak[4], Stanislav Jeleň[5], Beata Marciniak-Maliszewska[6], Petras Jokubauskas[7]

[1] *AGH University of Krakow, Faculty of Geology, Geophysics and Environment Protection, Krakow, Poland, e-mail: goleb@agh.edu.pl (corresponding author), ORCID ID: 0000-0002-4103-1124*
[2] *Przedsiebiorstwo Geologiczne S.A., Krakow, Poland, e-mail: natalia.ch255@gmail.com, ORCID ID: 0009-0003-7346-720X*
[3] *AGH University of Krakow, Faculty of Geology, Geophysics and Environment Protection, Krakow, Poland, e-mail: wlodek@agh.edu.pl, ORCID ID: 0000-0002-4954-1786*
[4] *Institute of Geophysics, Polish Academy of Sciences, Warsaw, Poland, e-mail: monika.kusiak@igf.edu.pl, ORCID ID: 0000-0003-2042-8621*
[5] *Matej Bel University, Faculty of Natural Sciences, Department of Geography and Geology, Banská Bystrica, Slovak Republic, e-mail: stanislav.jelen@umb.sk, ORCID ID: 0000-0002-1356-5209*
[6] *University of Warsaw, Faculty of Geology, Warsaw, Poland, e-mail: b.maliszewska@uw.edu.pl, ORCID ID: 0000-0001-9147-6693*
[7] *University of Warsaw, Faculty of Geology, Warsaw, Poland, e-mail: p.jokubauskas@uw.edu.pl, ORCID ID: 0000-0002-1099-4497*

Received: 10 June 2025; accepted: 11 September 2025; first published online: 30 September 2025

Abstract: Rare earth element (REE) mineralization has been documented at Rędziny, located on the eastern margin of the Karkonosze granite (Sudetes, Poland). Minerals of the REE[$(As,P)O_4$] group with a tetragonal zircon-type structure, primarily xenotime-(Y)-chernovite-(Y), $Y(PO_4)$-$Y(AsO_4)$ solid solutions, have been identified. These minerals occur as euhedral grains and also as intergrowths with secondary arsenates and silicates, filling cracks, fractures, and voids. Their textural diversity and paragenetic relationships with Ca-, Cu-, Pb-, and Bi-bearing arsenates indicate a crystallization sequence involving successive mineral-forming episodes. Local enrichments in REEs have also been recorded in common supergene arsenates, such as Ca(Pb)-Cu phases including conichalcite ($CaCu(AsO_4)(OH)$) and duftite ($PbCu(AsO_4)(OH)$). Minerals of the xenotime-(Y)-chernovite-(Y) solid solution correspond to intermediate compositions, with the chernovite end-member molar fraction ranging from 0.46 to 0.89. Based on EPMA analyses, yttrium is the dominant cation, accompanied by considerable amounts of middle rare earth elements (MREEs), especially neodymium (up to 12.60 wt.%; 0.21 apfu), samarium (up to 10.39 wt.%; 0.167 apfu), and gadolinium (up to 6.72 wt.%; 0.107 apfu). Some chemical compositions also show a trend towards the gasparite-(LREE) ($LREE(AsO_4)$) compositional field. Xenotime-(Y)-chernovite-(Y) minerals display microporosity, likely resulting from dissolution, metasomatic alteration, and subsequent recrystallization. The REEs at Rędziny likely originated from both evolved, late-stage hydrothermal fluids and rocks of the metamorphic envelope of the Karkonosze granite, where REEs were mobilized by post-magmatic fluids. Subsequent supergene processes may have further enhanced secondary enrichment.

Keywords: REE-bearing minerals, xenotime-(Y), chernovite-(Y), solid-solution, alteration

INTRODUCTION

Rare earth elements (REEs) consist of 15 lanthanides (La-Lu), often considered together with yttrium (Y) and Sc due to their similar chemical and ionic characteristics. They typically occur in the +3 oxidation state, show strong affinity for oxygen, and can easily substitute each other in mineral structures. Although yttrium is not a lanthanide, it commonly occurs with heavy rare earth elements (HREEs). The REEs and Y are essential for modern technologies because of their unique magnetic, luminescent and catalytic properties. They are widely used in electronics, renewable energy, and "green economy" applications, such as wind turbines, electric vehicles, etc. Their growing industrial demand and limited availability make them critical raw materials, especially in the context of sustainable technological development (e.g., Balaram 2019).

The main natural sources of REEs are minerals such as bastnäsite-(REE) and monazite-(REE), however less common REE-rich minerals are also important for understanding their geochemistry. Studying their occurrence, mineral associations, and genetic relationships is crucial for understanding the geochemical mobility and partitioning of REEs in different geological environments. Representative examples include REE-bearing arsenates and phosphates, which may crystallize from hydrothermal fluids or form as secondary phases during the weathering of primary REE-bearing minerals. Our study presents a less common case in which these REE minerals occur within the advanced weathering zone of hydrothermal ore mineralization, hosted in the envelope of a granite intrusion.

Minerals of $A[TO_4]$ structural group include phosphates and arsenates, where the A-site is typically occupied by REEs, with possible substitutions by Ca^{2+} and other divalent or trivalent cations. The T-site is usually occupied by As^{5+} or P^{5+}, with minor Si^{4+} and V^{5+} substitutions. This group consists of the xenotime group and the monazite supergroup. Two solid-solution series are identified within them: (1) the monazite-(REE)-gasparite-(REE) series, with a monoclinic monazite-type structure, and (2) the xenotime-(Y)-chernovite-(Y) series, which has a tetragonal zircon-type structure (e.g., Graeser et al. 1973, Graeser & Schwander 1987, Vereshchagin et al. 2019, Pagliaro et al. 2022, 2024, Ondrejka et al. 2024).

According to Ni et al. (1995) the crystal structure of xenotime group minerals is composed of isolated TO_4 tetrahedra bonded with $(REE)O_8$ unit in 8-fold coordination. This structural configuration is conducive to the incorporation of heavy rare earth elements (HREEs) and yttrium. In specific physicochemical conditions, some middle rare earth elements (MREEs), such as Gd and Sm, may also be included. In contrast, monazite-group minerals are built of $(REE)O_9$ polyhedra, with REE cations occupying positions in 9-fold coordination. This higher coordination number permits the incorporation of larger REE cations, mainly the light rare earth elements (LREEs). As a result, monazite structures preferentially host La, Ce, Pr, and Nd, whereas xenotime structures are more suitable for Y, Gd, Dy, Yb, and other smaller-radius cations (e.g., Pagliaro et al. 2022).

The present study aims to characterize the xenotime-(Y)-chernovite-(Y) solid solution to shed more light on the elemental behavior of the REEs in a weathered zone. Understanding these processes is critical due to the growing demand for REEs.

GEOLOGICAL SETTINGS AND MATERIALS

The eastern margin of the Karkonosze-Izera Massif is a metamorphic zone located between the Variscan Karkonosze granite to the west and the Carboniferous-Permian Intrasudetic Basin to the east (Fig. 1). This belt mainly consists of gneisses, mica schists, and metabasites. These rocks have been investigated and interpreted in various ways by numerous authors (Berg 1913, Teisseyre 1971, 1973, Chaloupský 1965, 1989, Oberc 1965, Mazur 1995, Kryza & Mazur 1995). Based on Teisseyre's classical stratigraphic subdivision (1971, 1973), Kryza and Mazur (1995) identified four main lithostratigraphic units within this part of the massif: the Kowary Gneiss Group, the Czarnów Schist Formation, the Niedamirów Schist Formation, and the Leszczyniec Meta-igneous Complex.

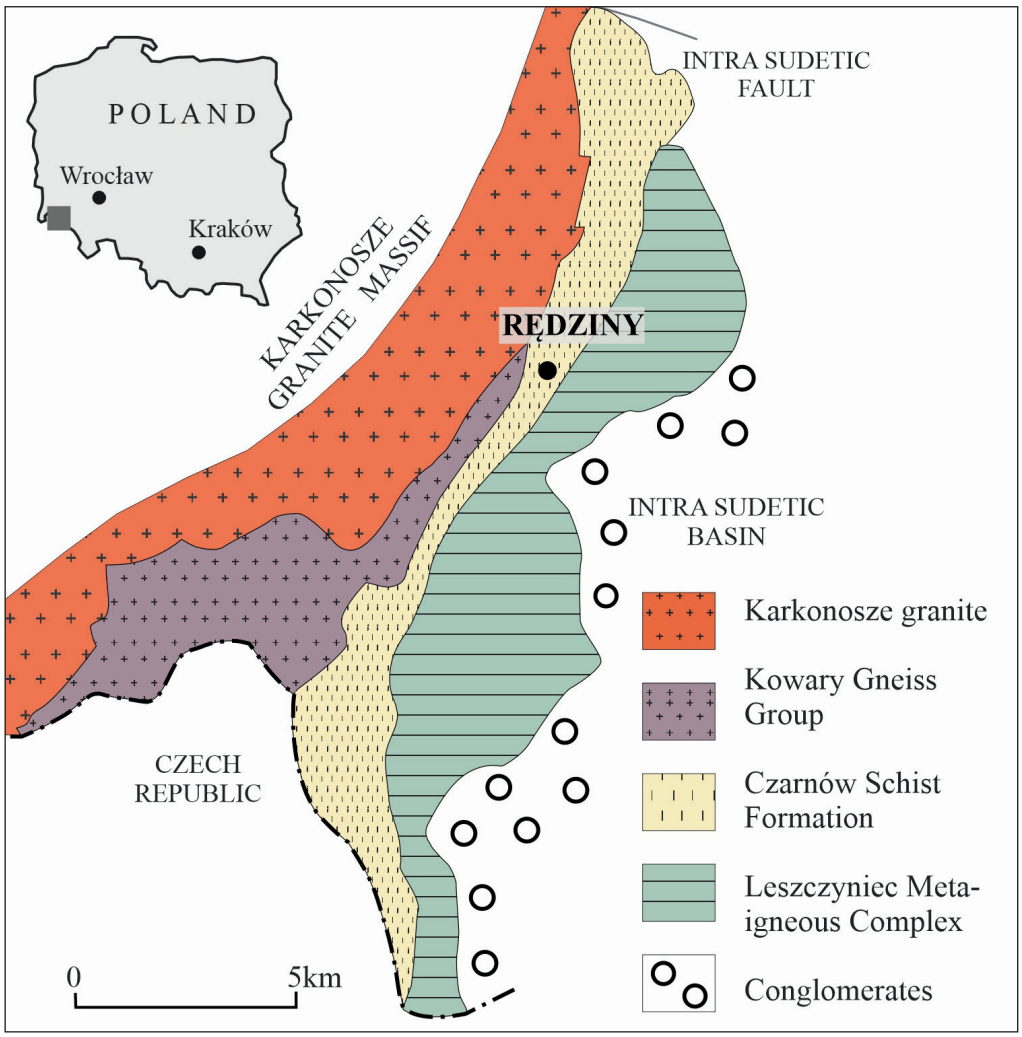

Fig. 1. *Simplified geological sketch of the eastern metamorphic margin of the Karkonosze Granite (after Teisseyre 1973, Mazur 1995)*

The protolith of the Kowary Gneiss has been dated from the latest Cambrian to earliest Ordovician (492–481 Ma, Oliver et al. 1993; 487 ±8 Ma, Oberc-Dziedzic et al. 2010). The associated quartz-feldspar schists, interlayered with the gneiss, have a similar sedimentation age. A closely related formation age is also suggested for the Czarnów Schist Formation. The Karkonosze pluton is late- to post-orogenic, high-K calc-alkaline, and peraluminous (A/CNK 1.01–1.1), classified as I-type to transitional I-S-type magma (Duthou et al. 1991, Mikulski 2007, Oberc-Dziedzic et al. 2009). The pluton was formed through the mixing of felsic and mafic magmas (Słaby & Martin 2008). It is comprised of three main granite types: porphyritic granite (coarse to medium-grained, biotite-bearing); equigranular granite (medium to fine-grained, found within porphyritic granite); granophyre granite (fine-grained, subordinate), with abundant lamprophyre and aplite dykes (Borkowska 1966). Lamprophyre and aplite dykes intruded the porphyritic granite, and hydrothermal recrystallization formed pegmatites (Kozłowski & Sachanbiński 2007). Pegmatite formation was aided by magma evolution together with enrichment of H_2O and other volatile elements (Mikulski 2007).

The age of the Karkonosze granite has been determined using various isotopic systems. Whole-rock Rb-Sr dating gave 328 ±12 Ma for central porphyritic granite and 309 ±3 Ma for ridge equigranular granite (Duthou et al. 1991). The U-Pb and

Pb-Pb zircon analyses indicated ages ranging 318–304 Ma (Kröner et al. 1994, Machowiak & Armstrong 2007, Kusiak et al. 2009, Kryza et al. 2014). To refine these results, monazite dating was used, providing 310–313 Ma for porphyritic and ca. 318 Ma for equigranular granite (Kusiak et al. 2014).

Tectonic processes associated with the emplacement of the Karkonosze granite have caused the formation of fracture zones and deformation structures in the surrounding rocks. These structures served as pathways for post-magmatic hydrothermal fluids, which played a key role in the development of polymetallic mineralization. This mineralization is widespread in the eastern metamorphic envelope of the granite, where it is mainly concentrated along faults and lithological contacts. Mining activity in this area dates back to the Middle Ages, with documented operations in the Miedzianka–Ciechanowice, Czarnów, and Kowary districts. The ore deposits in these areas were primarily enriched in Cu, Fe, Bi, As, Sb, Au, Ag, and U, with subordinate amounts of Te, Se, and various trace elements (Zimnoch 1978, Mochnacka et al. 2015). Notably, the presence of REE-bearing mineral phases and significant rare earth element enrichment has also been documented in the zone on the eastern margin of the granite. Secondary mineral assemblages in the mine dumps of the Miedzianka–Ciechanowice area have been described by several authors, who reported a paragenesis of REE arsenates, including agardite-(La) and plumboagardite (Siuda & Gołębiowska 2011).

Currently, extensive polymetallic mineralization is recorded in the active dolomite quarry at Rędziny. The dolomite lens is transected by NNW–SSE trending schist zone composed of mylonites, mica schists and amphibolites, which facilitated the migration of granite-derived hydrothermal fluids. The disseminated hydrothermal assemblage is dominated by minerals such as arsenopyrite, cassiterite, pyrite, sphalerite, pyrrhotite, tetrahedrite-group minerals, bismuthinite and complex Cu-, Ag-, Bi-, Pb-, and Sb-bearing sulphosalts, along with sulphotellurides, Sn-sulphides, bismuth, gold, and various other rare phases (e.g., Wołkowicz & Wołkowicz 1985, Parafiniuk & Domańska 2002, Parafiniuk et al. 2008, Pieczka et al. 2009, 2011, Gołębiowska et al. 2012).

The weathering of the primary sulphide assemblage has given rise to a well-developed oxidation zone, enriched in diverse secondary oxidized minerals. These are mainly arsenates and vanadates of mixed composition from the adelite-descloizite group, including species such as conichalcite (Cu-Ca arsenate, $CaCu(AsO_4)(OH)$), duftite (Cu-Pb arsenate, $PbCu(AsO_4)(OH)$), mottramite (Cu-Pb vanadate, $PbCu(VO_4)(OH)$), and (clino)tyrolite (Ca-Cu arsenate, $Ca_2Cu_9(AsO_4)_4(CO_3)(OH)_8 \cdot 11H_2O$), olivenite-adamite (Zn-Cu arsenate, $Cu_2(AsO_4)(OH)$-$Zn_2(AsO_4)(OH)$), philipsbornite (Pb-Al arsenate, $PbAl_3(AsO_4)(AsO_3OH)(OH)_6$), strashimirite (Cu arsenate, $Cu_4(AsO_4)_2(OH)_2 \cdot 2.5H_2O$), as well as iron arsenates (e.g., yukonite, $Ca_2Fe^{3+}_3(AsO_4)_3(OH)_4 \cdot 4H_2O$; scorodite, $Fe^{3+}(AsO_4) \cdot 2H_2O$; pharmacosiderite, $KFe^{3+}_4(AsO_4)_3(OH)_4 \cdot 6–7H_2O$).

Less commonly, phosphate minerals such as mimetite ($Pb_5(AsO_4)_3Cl$) and pyromorphite ($Pb_5(PO_4)_3Cl$) are also present (Parafiniuk 2003, Gołębiowska et al. 2006, 2016). The secondary paragenesis is additionally enriched by metal oxides, silicates, and carbonates, together with secondary bismuth and tellurium minerals, including bismite (Bi_2O_3) and eulytine ($Bi_4(SiO_4)_3$) (Fig. 2).

This contribution examines REE mineralization occurring within an extensive weathering zone in the Rędziny area. The mineralization is primarily represented by members of the xenotime-(Y)-chernovite-(Y) solid solution series, which exhibit a wide range of LREE-HREE substitutions and variable As-P ratios. The assemblage of these minerals also includes agardite-(REE), another rare arsenate. The REE-bearing phases typically occur as fine-grained aggregates, brittle crystals, occasionally reaching a few tenths of a micron in length. They frequently form porous accumulations that fill fractures, microcracks, and small cavities within mineral assemblages composed of Ca(Pb), Cu, and Zn arsenates, chrysocolla, malachite and iron oxides. These phases locally coexist with secondary bismuth minerals, including mixite, eulytine, and bismuth carbonates. However, more homogeneous, euhedral crystals of xenotime-(Y)-chernovite-(Y) have also been observed (Fig. 2C). Notably, local REE enrichment has been detected in coexisting conichalcite.

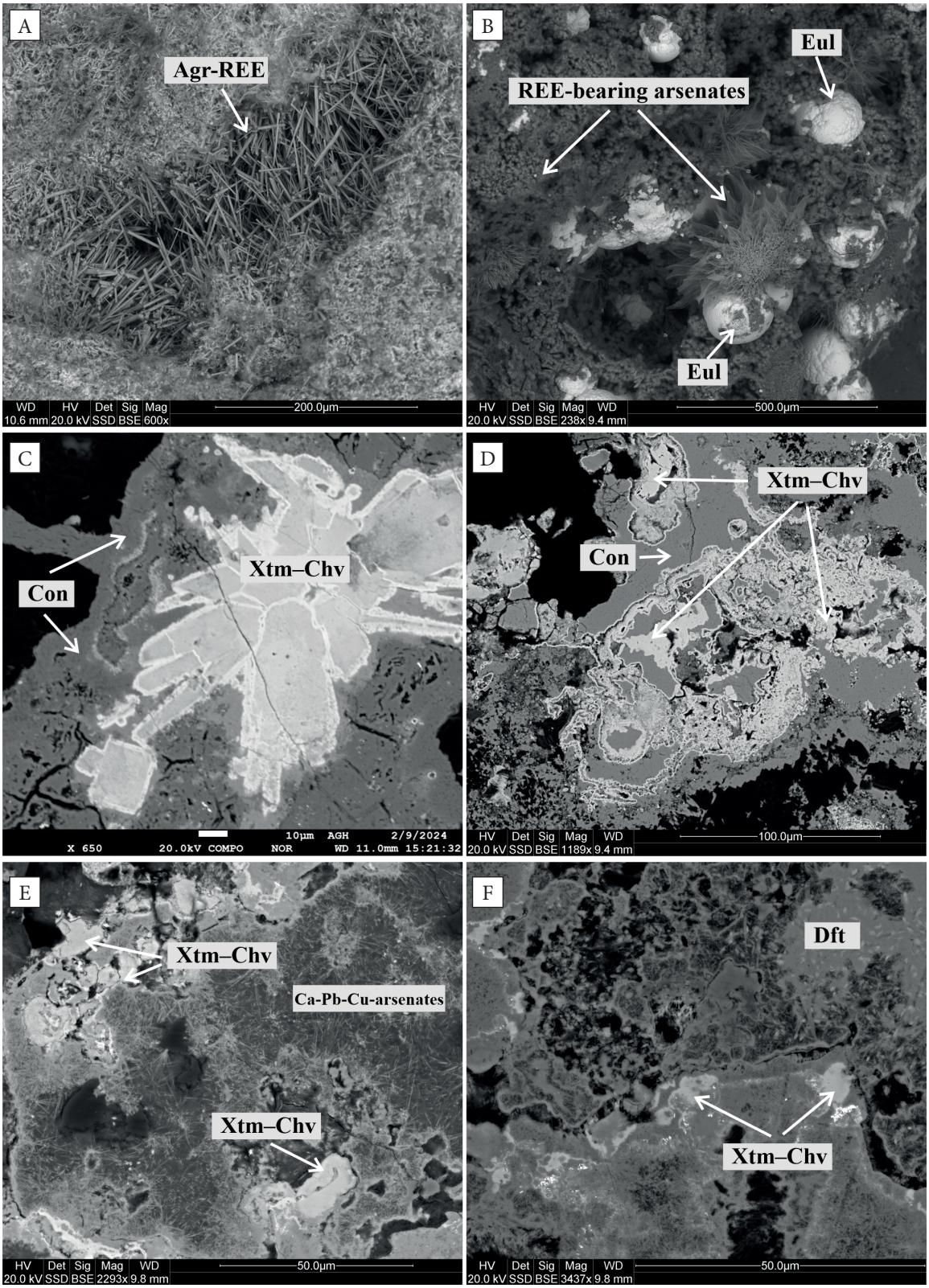

Fig. 2. *Mineral assemblages associated with weathering-related mineralization: A) acicular form of REE-agardite group minerals; B) spherulitic forms of eulytine occurring within REE-bearing arsenates; C) tetragonal and cube-like grains with rounded and smoothed forms, composed of the xenotime-(Y)-chernovite-(Y) solid solution (variations in contrast indicate differences REE distribution within the mineral grains); D)–F) intergrowths of xenotime-(Y)-chernovite-(Y) solid solution with common arsenates and other minerals typical of the oxidation zone. Mineral abbreviations after Warr (2021): Agr-REE – agardite-(REE), Con – conichalcite, Dft – duftite, Eul – eulytine, Xtm-(Y)-Chv-(Y) – xenotime-(Y)-chernovite-(Y) solid solution*

METHODS

Chemical analyses and elemental mapping were conducted in two laboratories using electron probe microanalysis (EPMA). Chemical composition of arsenates was obtained by means of electron probe microanalysis in the Laboratory of Electron Microscopy, Microanalysis and X-Ray Diffraction, Faculty of Geology, University of Warsaw. The analyses were carried out using a Cameca SX-100 Electron Probe Micro-Analyzer (EPMA) equipped with four wavelength dispersive spectrometers (WDS). Optimal conditions (a compromise between sample stability during electron beam interaction and measurement precision and accuracy) for EPMA of small arsenate crystals were set to a fully focused beam with 15 kV accelerating voltage and combined 8 nA (for major elements) and 15 nA (for traces) beam currents. The positions of individual background measurements, precise slope and interference corrections were thoroughly checked using HussariX (https://github.com/sem-geologist/HussariX), a free open-source tool for a wide range of WDS spectra collected with EPMA. The Φ(ρZ) correction model (X-PHI) developed by Merlet (1994), in conjunction with the built-in Cameca superset of mass attenuation coefficients, was used to quantify the chemical composition of the investigated minerals. Detailed information regarding EPMA analyses can be found in Table 1.

Table 1
Detailed information analyses by EPMA

Element measured	Analytical line	Diffracting crystal	Overlapping element	Reference material	Mean detection limit [ppm]	Beam current [nA]
F	Ka	PC0	Ce Mz, Pr Mz	Apatite-F	1050	8
Nd	La	LPET	Ce Lb	$NdPO_4$	1210	8
Ca	Ka	LPET	–	Diopside	380	8
As	La	TAP	Dy Ma	GaAs	1950	8
Y	La	TAP	–	YAG	1500	8
P	Ka	TAP	Ca Kb	$NdPO_4$	560	8
Na	Ka	PC0	–	Albite	640	8
Sm	La	LIF	Ce Lb2	$SmPO_4$	4200	8
Gd	La	LIF	Ce Lc, La Lc2	$GdPO_4$	4070	8
Dy	La	LIF	Mn Kb	$DyPO_4$	4700	8
Cu	Ka	LIF	–	Cuprite	2790	8
Ce	La	LPET	–	$CePO_4$	1210	8
U	Ma	LPET	–	UO_2	1610	8
Si	Ka	TAP	Nd La	Diopside	360	15
La	La	LPET	–	$LaPO_4$	710	15
Pr	La	LPET	La Lb	$PrPO_4$	680	15
Er	La	LIF	–	$ErPO_4$	3420	15
Yb	La	LIF	–	$YbPO_4$	3850	15
Tb	La	LIF	–	$TbPO_4$	3110	15
Ho	La	LIF	Gd Lb	$HoPO_4$	530	15
Eu	La	LIF	Nd Lb3, Pr Lb2	$EuPO_4$	2120	15
Tm	La	LIF	Sm Lc	$TmPO_4$	950	15
Lu	La	LIF	Dy Lb2, Ho Lb3	$LuPO_4$	740	15
Th	Ma	LPET	–	ThO_2	1080	15
Bi	Ma	LPET	Ce La	Bi_2Te_3	840	15
V	Ka	LIF	–	V_2O_5	1110	15
Zn	Ka	LIF	–	Sphalerite	2400	15
Mn	Ka	LIF	–	Rhodonite	1120	15
Fe	Ka	LIF	–	Fe_2O_3	1230	15

Elemental distribution measurements were performed using the JEOL JXA-8230 Electron Probe Micro-Analyzer located in the Laboratory of the Critical Elements at the Faculty of Geology, Geophysics and Environmental Protection, AGH University of Krakow. Elemental maps were made using the following parameters: accelerating voltage 15 kV, beam current 40 nA, dwell time 100 ms, and map frame size of 75.4 μm × 65.5 μm. The intensity of the characteristic X-ray lines listed below was measured using the following diffraction crystals: Kα order 1, PET (P, Y); Lα order 1, TAP (As); and Lα order 1, LIF (Ce, Nd, Sm, Gd, Dy, Er, Yb).

RESULTS AND DISCUSSION

Chemical compositions of the xenotime-(Y)-chernovite-(Y) solid solution from Rędziny

Representative results of chemical microprobe analyses of REE-bearing minerals are presented in order of increasing molar percent of the chernovite-(Y) end-member (Table 2). Analyses were carried out for REE[TO_4] phases forming intergrowths, vein-like fillings of fractures and cavities (Fig. 2D–F), as well as for euhedral grains (Fig. 2C).

Table 2
Representative microprobe analyses of chernovite-(Y)-xenotime-(Y) solid solution

Compound	Chemical data ordered by increasing molar content of chernovite-(Y) [wt.%]										Crystals with cubic habit [wt.%] (see Fig. 3)		
											rim	inter-mediate	core
	11_1a	1_1	2_1	12_1	9_1	4_1	3_1	15_1	11_1	10_1	21	7_22	7_21
As_2O_5	18.00	19.04	19.35	25.43	26.81	27.14	27.35	22.84	25.36	30.05	18.44	20.86	35.47
P_2O_5	13.19	11.79	11.22	9.28	6.19	6.04	5.88	4.72	4.60	3.91	13.07	12.00	2.81
SiO_2	1.04	0.95	0.95	0.58	0.83	0.75	0.57	2.59	2.15	0.31	4.02	2.84	0.88
V	0.16	0.00	0.53	0.36	0.14	0.12	0.31	0.01	0.29	0.22	0.34	0.33	0.21
UO_3	5.82	3.45	3.33	2.39	2.15	1.87	1.97	1.50	1.40	0.80	2.57	2.53	0.40
Bi_2O_3	0.13	b.d.	b.d.	0.22	0.18	b.d.	b.d.	0.37	0.33	0.24	b.d.	0.18	0.33
Y_2O_3	16.66	15.81	15.31	15.97	13.11	13.19	13.77	11.34	10.79	11.65	16.33	15.62	7.34
La_2O_3	0.06	0.15	0.15	0.19	0.26	0.25	0.17	0.21	0.22	0.19	0.10	0.16	0.33
Ce_2O_3	1.37	2.11	2.31	2.44	2.99	2.89	2.71	3.04	3.10	3.29	1.82	1.81	3.34
Pr_2O_3	0.66	0.10	1.04	0.10	1.22	1.25	1.20	1.35	1.41	1.35	0.79	1.03	1.24
Nd_2O_3	5.71	8.37	8.35	8.46	10.74	10.60	10.33	11.10	12.60	11.32	6.67	7.66	12.46
Sm_2O_3	7.12	8.16	8.55	7.48	9.00	8.900	8.88	9.98	10.39	8.34	6.76	7.09	9.34
Eu_2O_3	0.71	0.83	1.00	0.82	0.72	0.84	0.70	0.79	0.92	0.71	0.83	0.55	0.70
Gd_2O_3	5.65	6.36	6.10	5.49	6.10	6.38	5.89	6.72	6.44	5.41	5.45	6.13	5.93
Tb_2O_3	0.98	0.88	0.90	0.59	0.67	0.92	0.90	1.09	0.88	0.83	0.94	0.42	0.49
Dy_2O_3	5.13	4.94	4.94	4.21	4.98	4.52	4.32	4.77	4.39	3.68	5.02	4.10	3.50
Ho_2O_3	0.43	0.51	0.51	0.65	0.26	0.44	0.37	0.63	0.80	0.25	0.74	0.33	0.41
Er_2O_3	1.81	1.73	1.69	1.48	1.47	1.51	1.75	1.42	1.64	1.57	2.12	1.86	1.43
Tm_2O_3	0.35	0.07	0.14	0.31	0.19	0.37	0.30	0.35	0.36	0.18	0.25	0.27	0.36
Yb_2O_3	1.12	1.01	0.97	1.33	0.96	1.03	0.83	0.62	0.72	0.93	1.31	1.03	0.63
Lu_2O_3	0.22	0.18	0.23	0.08	b.d.	0.00	0.00	0.18	b.d.	0.21	0.00	0.14	b.d.
CaO	4.37	3.70	3.57	3.47	2.49	2.60	2.75	2.50	2.24	2.88	3.96	4.01	2.81
MnO	b.d.	0.15	b.d.	0.17	b.d.	b.d.	b.d.	b.d.	b.d.	b.d.	b.d.	b.d.	b.d.
FeO	0.42	0.26	0.25	b.d.	0.19	b.d.	b.d.	0.53	b.d.	0.28	b.d.	b.d.	b.d.
CuO	4.44	2.04	2.08	2.76	1.18	1.23	1.40	3.74	3.57	1.82	2.49	1.91	2.21

Table 2 *cont.*

Compound	Chemical data ordered by increasing molar content of chernovite-(Y) [wt.%]										Crystals with cubic habit [wt.%] (see Fig. 3)		
											rim	inter-mediate	core
	11_1a	**1_1**	**2_1**	**12_1**	**9_1**	**4_1**	**3_1**	**15_1**	**11_1**	**10_1**	**21**	**7_22**	**7_21**
ZnO	0.77	0.87	0.71	0.92	0.45	0.58	0.36	0.94	0.82	0.52	0.91	0.55	0.62
F	0.32	0.45	0.40	0.35	0.25	0.12	0.15	0.24	0.15	b.d.	0.23	0.21	b.d.
$O=F_2$	0.13	0.19	0.17	0.15	0.11	0.05	0.06	0.10	0.06	0.00	0.10	0.09	0.00
Total	96.51	93.72	94.41	95.38	93.42	93.50	92.80	93.47	95.51	90.94	95.06	93.53	93.24
Chemical formula based on 4 (O + F) [pfu]													
T-site													
As	0.397	0.437	0.445	0.573	0.650	0.659	0.666	0.571	0.620	0.756	0.392	0.456	0.858
P	0.471	0.438	0.417	0.339	0.243	0.238	0.232	0.191	0.182	0.159	0.450	0.425	0.110
Si	0.044	0.042	0.042	0.025	0.038	0.035	0.027	0.124	0.101	0.015	0.164	0.119	0.041
V	0.004	0.000	0.015	0.010	0.004	0.004	0.010	0.000	0.009	0.007	0.009	0.009	0.006
ΣT-site	0.916	0.917	0.919	0.947	0.935	0.936	0.935	0.886	0.912	0.937	1.015	1.009	1.015
A-site													
U^{6+}	0.052	0.032	0.031	0.022	0.021	0.018	0.019	0.015	0.014	0.008	0.022	0.022	0.004
Bi^{3+}	0.001	0.000	0.000	0.002	0.002	0.000	0.000	0.005	0.004	0.003	0.000	0.002	0.004
Y^{3+}	0.374	0.370	0.358	0.366	0.323	0.326	0.341	0.289	0.269	0.299	0.354	0.348	0.181
La^{3+}	0.001	0.002	0.002	0.003	0.004	0.004	0.003	0.004	0.004	0.003	0.002	0.002	0.006
Ce^{3+}	0.021	0.034	0.037	0.038	0.051	0.049	0.046	0.053	0.053	0.058	0.027	0.028	0.057
Pr^{3+}	0.010	0.002	0.017	0.002	0.021	0.021	0.020	0.024	0.024	0.024	0.012	0.016	0.021
Nd^{3+}	0.086	0.131	0.131	0.130	0.178	0.176	0.172	0.190	0.210	0.195	0.097	0.114	0.206
Sm^{3+}	0.103	0.124	0.129	0.111	0.144	0.142	0.143	0.165	0.167	0.138	0.095	0.102	0.149
Eu^{3+}	0.010	0.012	0.015	0.012	0.011	0.013	0.011	0.013	0.015	0.012	0.012	0.008	0.011
Gd^{3+}	0.079	0.093	0.089	0.078	0.094	0.098	0.091	0.107	0.100	0.086	0.074	0.085	0.091
Tb^{3+}	0.014	0.013	0.013	0.008	0.010	0.014	0.014	0.017	0.014	0.013	0.013	0.006	0.007
Dy^{3+}	0.070	0.070	0.070	0.058	0.074	0.068	0.065	0.074	0.066	0.057	0.066	0.055	0.052
Ho^{3+}	0.006	0.007	0.007	0.009	0.004	0.007	0.005	0.010	0.012	0.004	0.010	0.004	0.006
Er^{3+}	0.024	0.024	0.023	0.020	0.021	0.022	0.026	0.021	0.024	0.024	0.027	0.024	0.021
Tm^{3+}	0.005	0.001	0.002	0.004	0.003	0.005	0.004	0.005	0.005	0.003	0.003	0.004	0.005
Yb^{3+}	0.014	0.014	0.013	0.017	0.014	0.015	0.012	0.009	0.010	0.014	0.016	0.013	0.009
Lu^{3+}	0.003	0.002	0.003	0.001	0.000	0.000	0.000	0.003	0.000	0.003	0.000	0.002	0.000
Ca^{2+}	0.197	0.174	0.168	0.160	0.124	0.129	0.137	0.128	0.112	0.149	0.173	0.180	0.139
Mn^{2+}	0.000	0.006	0.000	0.006	0.000	0.000	0.000	0.000	0.000	0.000	0.000	0.000	0.000
Fe^{2+}	0.015	0.010	0.009	0.000	0.007	0.000	0.000	0.021	0.000	0.011	0.000	0.000	0.000
Cu^{2+}	0.141	0.068	0.069	0.090	0.041	0.043	0.049	0.135	0.126	0.066	0.077	0.060	0.077
Zn^{2+}	0.024	0.028	0.023	0.029	0.015	0.020	0.012	0.033	0.028	0.018	0.027	0.017	0.021
ΣA-site	1.25	1.217	1.209	1.166	1.162	1.17	1.17	1.321	1.257	1.188	1.107	1.092	1.067
ΣREE	0.820	0.899	0.909	0.857	0.952	0.960	0.953	0.984	0.973	0.933	0.805	0.812	0.821
O^{2-}	3.958	3.937	3.944	3.952	3.978	3.982	3.963	3.978	3.964	4.000	3.97	3.972	4.000
F^-	0.042	0.063	0.056	0.048	0.022	0.018	0.037	0.022	0.036	0.000	0.030	0.028	0.000
As/(As+P)	0.46	0.50	0.52	0.63	0.73	0.74	0.74	0.75	0.77	0.83	0.47	0.52	0.89

b.d. – below detection; As/(As+P) – atomic ratio.

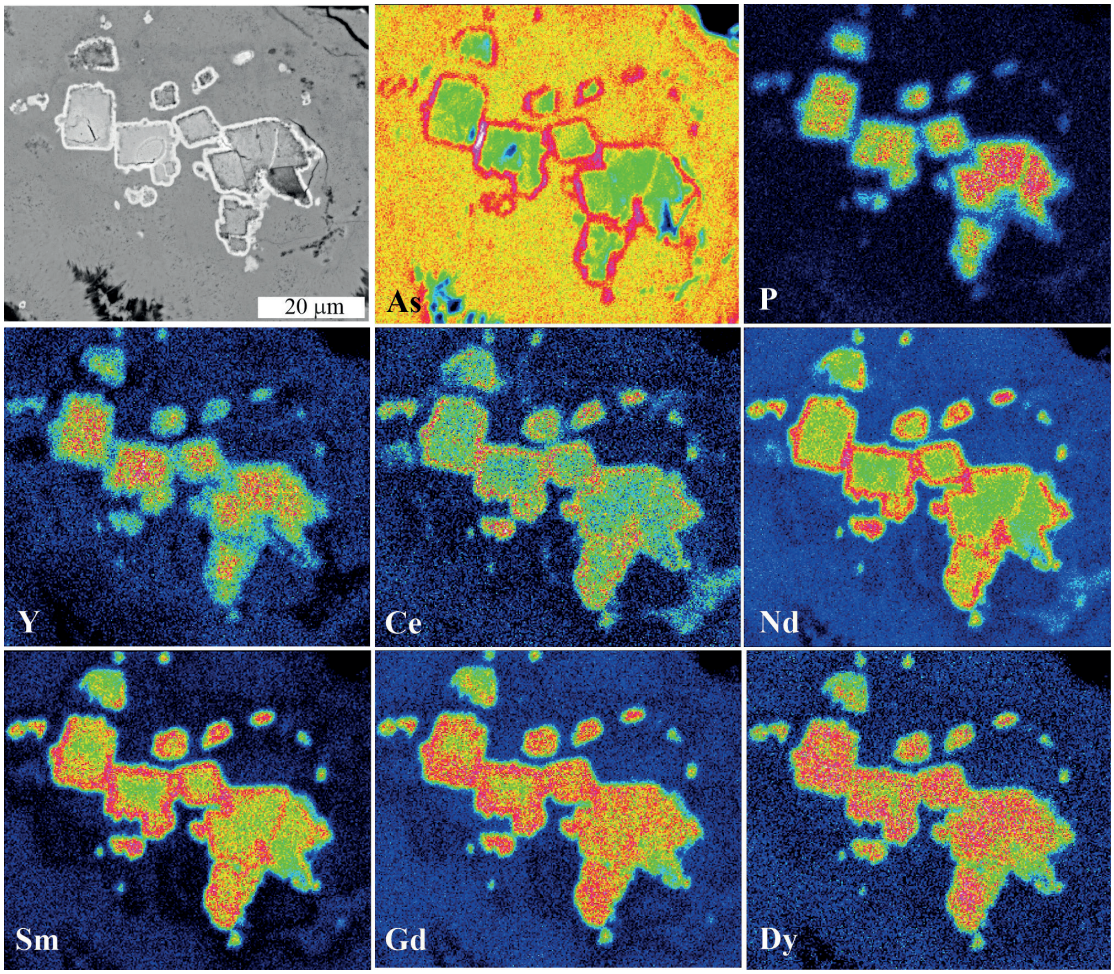

Fig. 3. *Element mapping of tetragonal grains from the xenotime-(Y)-chernovite-(Y) solid solution, obtained by EPMA. Color scale of increasing concentrations of the elements: dark blue–blue–green–yellow–orange–red–purple–white*

Analytical points were selected based on BSE contrast and the highest observed grain homogeneity. Additional EPMA elemental distribution maps were acquired for the tetragonal crystals shown in Figure 3.

Analytical totals range 90–95 wt.%, which is attributed to the nanoporous character of the structures, as shown in Figure 2D–F. More homogeneous grains observed in BSE images give more exact analytical totals in weight percent.

In ideal chernovite-(Y), [$Y(AsO_4)$], the total content of Y_2O_3 and REE_2O_3 exceeds 51 wt.%, with Y_2O_3 reaching up to 44 wt.%. In contrast, in xenotime-(Y) [$Y(PO_4)$], the Y_2O_3 content typically exceeds 61 wt.%. In the analyzed samples, Y_2O_3 content ranges 7.34–16.66 wt.% (0.18–0.37 apfu), while the total Y + REE content varies 47.50–54.66 wt.%. The total content of lanthanide oxides (ΣREE) ranges 31.26–43.87 wt.%.

Among the REEs, the dominant elements are MREEs Nd, Sm, and Gd, with concentrations ranging 5.71–12.60 wt.% (0.08–0.21 apfu), 6.76–10.39 wt.% (0.09–0.17 apfu), and 5.45–6.72 wt.% (0.01–0.1 apfu), respectively. Dy is also an important element, with a content ranging 3.50–5.13 wt.% (0.05–0.07 apfu). In some cases, slightly elevated concentrations of LREEs (e.g., Ce_2O_3 up to 3.34 wt.%; 0.06 apfu) compared to HREEs (e.g., Er_2O_3 up to 2.12 wt.%, 0.03 apfu) are observed. As shown in the ternary diagram (Fig. 4), atomic proportions of Nd, Sm, and Gd reveal that Nd and Sm are the dominant components in the analyzed crystals. It should be noted, however, that Y shows the highest atomic proportion among REE cations, even though the total amount of all REEs exceeds that of Y.

The analyzed grains are primarily arsenate compositions, with a molar chernovite end-member ranging from 0.46 to 0.89. Figure 5 shows the

P-As substitution trend, with a negative correlation between the components. Silicon is subordinate, with values between 0.015 and 0.163 apfu, and vanadium is present in trace amounts below 0.015 apfu. Figure 6B, C display substitution trends between As and Y, P and Y. Yttrium and arsenic exhibit a negative correlation. In contrast, phosphorus correlates positively with Y, suggesting the preferential incorporation of Y into phosphate-rich phases. This distribution corresponds to the geochemical behavior of Y under acidic conditions favoring phosphate stability.

The chemical composition of the analyzed minerals also reveals the presence of Ca, Cu, Zn, Fe, Bi, U, and several other minor elements. The highest concentrations are observed for CaO and CuO, ranging 2.24–4.37 wt.% (0.11–0.19 apfu) and 1.18–4.44 wt.% (0.04–0.14 apfu), respectively. ZnO contents reach up to 1 wt.%, while FeO, MnO, and Bi_2O_3 are present at levels below 0.5 wt.%. Ti, Th, and Zr were below the detection limit. Notably, UO_3 concentrations are relatively high, reaching up to 5.82 wt.% (0.05 apfu) in some spots (see Table 2).

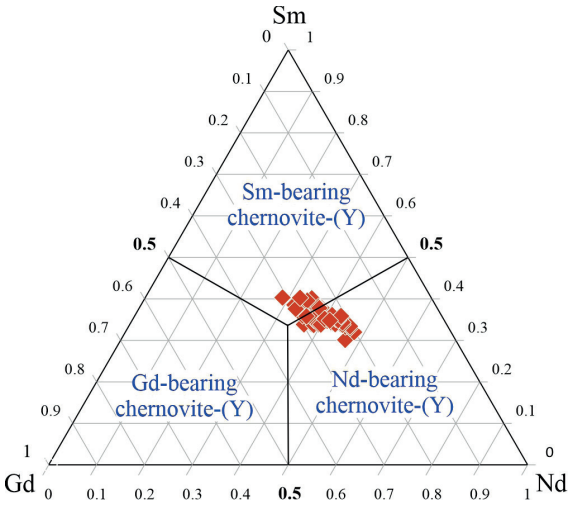

Fig. 4. Ternary projection of Sm-Nd-Gd contents [apfu] in the xenotime-(Y)-chernovite-(Y) solid solution from Rędziny

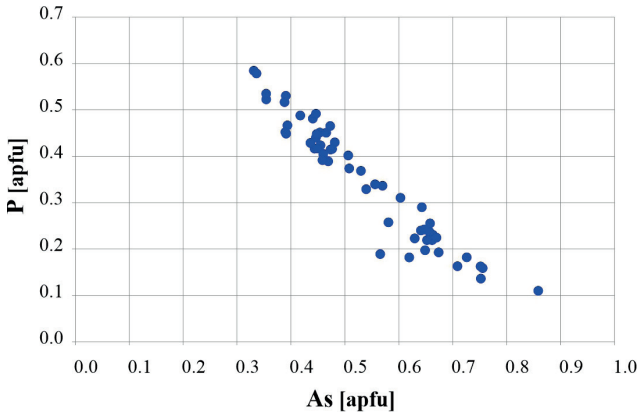

Fig. 5. Correlation plot of phosphorus vs. arsenic in the xenotime-(Y)-chernovite-(Y) solid solution from Rędziny

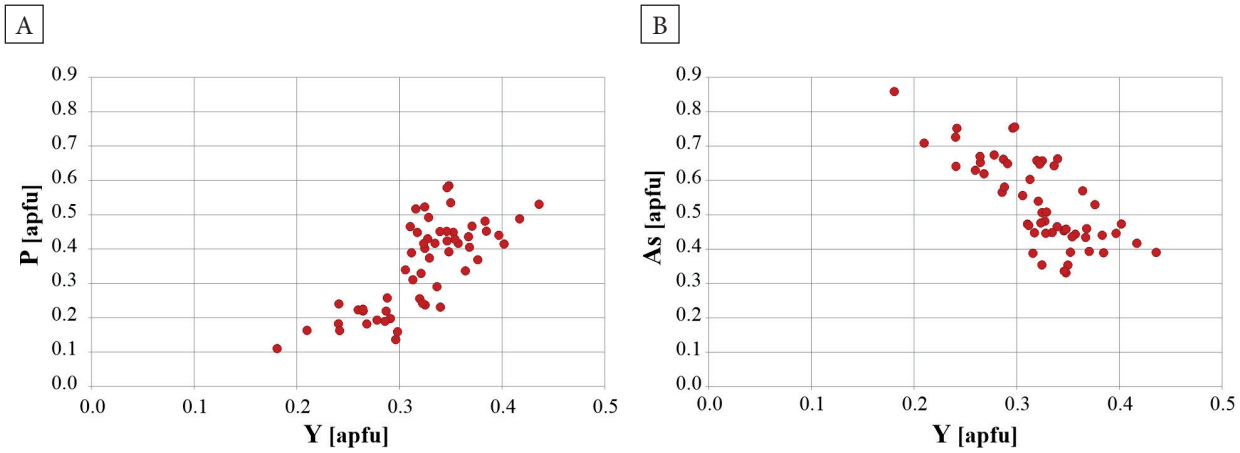

Fig. 6. Correlation plots of selected components in the xenotime-(Y)-chernovite-(Y) solid solution: A) phosphorus vs. yttrium; B) arsenic vs. yttrium

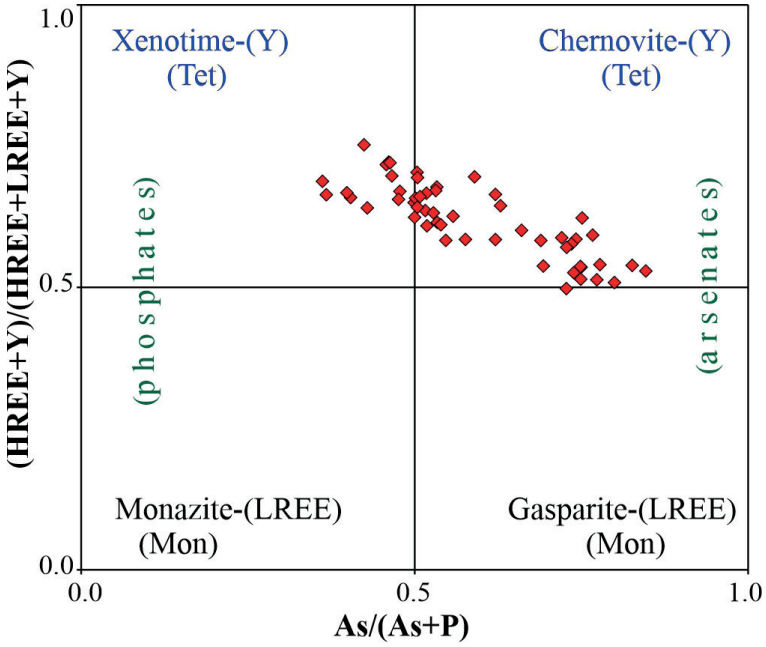

Fig. 7. *Chemical compositions of REE minerals from Rędziny, shown in the (Y+REE)[AsO_4]–(Y+REE)[PO_4] system proposed by Ondrejka et al. (2007); Tet – tetragonal; Mon – monoclinic*

Figure 7 shows compositional data from Rędziny samples plotted within the (Y,REE)[AsO_4]–(Y,REE)[PO_4] quadrilateral, where the analyzed grains fall within the xenotime-(Y)-chernovite-(Y) solid solution range, but are often shifted towards the chernovite-(Y)-gasparite-(REE) compositional boundary. Compared to known gasparite-(REE) species, which are typically La- or Ce-dominant, the Rędziny samples are enriched in Nd and Sm. This indicates a clear enrichment in LREEs within the arsenate members.

The analytical totals of the REE[TO_4] minerals from Rędziny range 90–95 wt.%. This deficit is attributed to microporosity, likely formed during intense mineral dissolution, metasomatic alteration, and the subsequent reprecipitation of chernovite-(Y). According to Förster et al. (2011), similar analytical totals were interpreted as indicating hydrated xenotime-(Y)-chernovite-(Y) solid solutions. However, we interpret these phases as altered rather than hydrated. The observed porosity suggests leaching-related processes, during which more mobile elements were released from the primary structure followed by later stage recrystallization. Tetragonal xenotime-(Y)-chernovite-(Y) crystals, especially their outlines, show chemical composition variations visible as contrast differences in BSE images. These grains often display rounded, smoothed forms (Figs. 2, 3), indicating dissolution processes. Their surfaces are heterogeneous, reflecting variable composition and degrees of alteration. Figures 2 and 3 show such grains with rims developed in the outermost zones. The grains are embedded in arsenates and other common secondary phases, which are often amorphous and chemically non-stoichiometric. Chemical mapping of tetragonal xenotime-(Y)-chernovite-(Y) forms showed a negative correlation between arsenic and phosphorus. Phosphorus is concentrated in the crystal cores, while the outer zones – especially the rims – are enriched with arsenic. A similar distribution is observed for HREEs, which concentrate in the inner parts of the crystals together with Y. In contrast, LREEs tend to accumulate near the crystal rims.

Mineralogy and crystal chemistry: background and new data

Arsenate members of the REE[TO_4] group are significantly less common in natural systems compared to their phosphate analogues. Therefore, experimental studies on the stability of these

compounds have primarily focused on phosphate phases (e.g., Kolitsch & Holtstam 2004a, 2004b). Chernovite-(Y), although a rare yttrium arsenate, has been reported from natural occurrences associated with post-magmatic hydrothermal and pegmatitic mineralization, or with autometasomatic alteration of xenotime-(Y) in granitic rocks (Zinnwald, Eastern Erzgebirge, Germany; Förster et al. 2011), rhyolitic rocks (Tisovec-Rejkovo, Western Carpathians, Slovakia; Ondrejka et al. 2007), quartz-bearing fissures related to pegmatites from Mt. Cervandone (Western Alps, Piedmont, Italy; Pagliaro et al. 2022), and rare-metal granites and greisens of the Far East (Alekseev & Marin 2013). In contrast, only a few studies have documented chernovite-(Y) formation in oxidation ore zones, e.g., in the Vorontsovskoe gold deposit (Northern Urals; Kasatkin et al. 2022), and in regolith-hosted HREE deposits, exemplified by the Zudong deposit in Jiangxi Province, South China (Li et al. 2019).

In the ideal composition of the xenotime-(Y)-chernovite-(Y) solid solution, $A[(P,As)O_4]$, the A-site is occupied mainly by yttrium. However, natural chernovite-(Y) samples often show significant substitution by other REEs, including both LREE and HREE representatives (e.g., Cabella et al. 1999, Ondrejka et al. 2007, Förster et al. 2011, Pagliaro et al. 2022, 2024). After Pagliaro et al. (2024) the presence of REEs into this position depends on ionic radius. Larger cations such as La, Ce, and Nd tend to stabilize the monoclinic monazite-type structure ($P2_1/n$), while smaller ions like Y, Gd-Lu, and Sc are more compatible with the tetragonal zircon-type structure ($I4_1/amd$) typical of xenotime-(Y) and chernovite-(Y).

The stability of these structures also depends on the metal occupying the tetrahedral site of the crystal structure. High As/P ratios tend to promote the crystallization of zircon-type minerals, which preferentially accommodate HREEs, while phosphate dominated compositions favour LREE-bearing monazite-type structures (e.g., Kolitsch & Holtstam 2004a, 2004b, Ondrejka et al. 2007). According to Pagliaro et al. (2024), in phosphate systems, the monazite-zircon structural boundary occurs near Sm or Gd. The larger ionic radius of As^{5+} compared to P^{5+} increases the volume of the tetrahedral site, allowing slightly larger REEs to be incorporated in zircon-type structures. As a result, even Sm and occasionally Nd can be stabilized in tetragonal arsenate frameworks (e.g., Pagliaro et al. 2024). This indicates that crystal chemistry controls the partitioning of REEs during mineral formation. In the analyzed chernovite-(Y) samples from Rędziny, the dominant REEs are Sm, Nd, and Gd. Although Nd is generally associated with monazite-type minerals due to its relatively large ionic radius, it reaches up to 12.46 wt.% Nd_2O_3 (0.21 apfu) in the analyzed samples. Similarly, Förster et al. (2011) observed high Nd_2O_3 contents up to 9.5 wt.% in hydrated chernovite-type phases. These findings demonstrate that zircon-type structures can incorporate mid-sized REEs like Nd^{3+} under favorable geochemical conditions. Experimental results by Feigelson (1967) further confirm this structural tolerance. By partially substituting Nd^{3+} with smaller Sm^{3+}, zircon-type $Nd_{0.65}Sm_{0.35}AsO_4$ crystals were synthesized, supporting the idea that mixed-REE occupancy can shift structural preferences toward the tetragonal field. This anion-controlled substitution explains the formation of Nd-, Sm-, and Gd-enriched chernovite in both supergene weathering zones and low-temperature hydrothermal environments (Feigelson 1967). Overall, these findings indicate that the tetragonal structure of chernovite is more chemically variable than previously assumed. Elements such as Nd, Sm, and Gd are valuable indicators of structural evolution and REE behavior in arsenate-dominated systems.

Formation of REE-bearing minerals

It can be assumed that the grains shown in Figures 2 and 3 originally precipitated from primary post-magmatic fluids and were subsequently modified by metasomatic alteration and partial dissolution. These processes may have been initiated by the breakdown of primary sulphides and the influence of an acidic, aggressive environment. The presence of arsenopyrite as the main ore mineral in the Rędziny assemblage shows that the hydrothermal fluids were rich in arsenic. Arsenic also occurs in lower-temperature minerals from the tetrahedrite group. The breakdown of these minerals, together with oxidizing conditions, changed the composition of circulating fluids, further

enriched them in arsenic, and led to the crystallization of secondary arsenates. Additionally, elemental distribution maps (Fig. 3) reveal distinct contrast within individual grains. Phosphorus, Y, and HREEs are concentrated in the inner parts of the crystals, while the outer zones show enrichment in arsenic and LREEs/MREEs. This distribution can be attributed to the fractionation of REEs during mineral crystallization (Migdisov et al. 2019). Heavy REEs tend to crystallize earlier and become incorporated into phosphate structures such as xenotime-(Y). The enrichment of MREEs and LREEs in the outer zones may also reflect variations in element mobility during the alteration of crystals within the xenotime-(Y)-chernovite-(Y) solid solution. Phosphorus and HREEs are less mobile, whereas arsenic and LREEs, being more mobile, tend to concentrate in the peripheral zones. This suggests partial dissolution of previously existing phosphate-rich members, followed by recrystallization of chernovite-(Y) enriched in light REEs in the marginal zones of the grains. Similar observations were made by Gorelikova et al. (2022). The source of the REEs in Rędziny may be of dual origin. On the one hand, they could have been concentrated in late-stage, evolved, and highly mineralized hydrothermal fluids. On the other hand, REEs may have been derived from rocks of the metamorphic envelope of the granite, where they were mobilized by infiltrating F-, Cl-, and OH-bearing fluids. This process led to the secondary enrichment of late-stage fluids migrating along tectonic fractures. This mechanism was proposed by Mil et al. (2024) in a study on the sources of REEs in postmagmatic mineralization observed in the central part of the Karkonosze granite near Szklarska Poręba. Phosphate minerals are much less common than arsenates in the Rędziny area, as well as in other weathering zones within the eastern metamorphic envelope of the granite. The crystallization of arsen-rich phases was likely caused by the dominance of arsenate ions in circulating secondary fluids. However, apatite was found in mylonitized zones at Rędziny and may have been a source of both phosphorus and REEs. In acidic conditions, apatite becomes more soluble and could have released these elements into the surrounding fluids during weathering. In the advanced weathering zone at Rędziny, also identified agardite-(REE) and non-stoichiometric arsenates containing up to 20 wt.% UO_3, along with significant concentrations of REEs. The occurrence of these phases indicates the co-mobility of uranium and REEs under oxidizing conditions. In studied members of the xenotime-(Y)-chernovite solid solution series, a positive correlation between uranium and phosphorus was observed, suggesting a common remobilization mechanism. A comparable case was documented by Syczewski et al. (2022), who reported REE and uranium enrichment in phosphate and arsenate minerals formed within weathering environments at the Podgórze mine near Kowary. The presence of carbonate rocks at Rędziny is also significant – the leaching of calcium and magnesium ions may have locally elevated the pH, thereby promoting the stabilization of $REE(TO_4)$ phases through the incorporation of Ca^{2+} into their crystal structure.

CONCLUSIONS

An important mineralogical observation is the presence of REE minerals representing the xenotime-(Y)-chernovite-(Y) solid solution in a highly developed weathering zone. These minerals show a wide range of isomorphic substitutions, including significant LREE-HREE variability and variable As-P ratios. This suggests dynamic changes in physicochemical conditions during their crystallization – particularly variations in pH, redox potential (Eh), and the activity of metal ions in circulating hydrothermal and supergene fluids.

The chemical composition of the Rędziny samples confirms the existence of a solid solution between tetragonal xenotime-(Y) and chernovite-(Y). Most of the compositions are arsenate-dominant, and there is a clear trend toward the boundary with gasparite-(REE). In comparison to monoclinic arsenates from the monazite group, the grains from Rędziny contain more Nd and Sm.

Xenotime-chernovite solid solution members from Rędziny show evidence of secondary alteration. The euhedral crystals exhibit variable chemical composition, as revealed by BSE imaging, showing variation from the core to the outermost zones.

The inner parts of the grains are clearly enriched in phosphorus and HREEs, which is interpreted as (i) a result of their lower mobility compared to arsenic and LREEs, and (ii) metasomatic processes involving dissolution and mineral decomposition. The REEs in the Rędziny weathering zone were likely derived from both late-stage, evolved hydrothermal fluids and rocks of the metamorphic envelope of the granite, where they were mobilized by circulating fluids.

We are very grateful to the Reviewers whose comments have greatly improved the manuscript. We would like to extend our thanks to Prof. Adam Pieczka for checking the chemical recalculations. This study was supported by the AGH University of Krakow grant 16.16.140.315. The research project was partly supported by the program "Excellence initiative – research university" for the AGH University of Krakow.

REFERENCES

Alekseev V.I. & Marin Y.B., 2013. A tribute to Nicolai Pavlovich Yushkin, one of the discoverers of chernovite. Chernovite-(Y) and other arsenic minerals in rare-metal granites and greisens of the Far East. *Geology of Ore Deposits*, 55(7), 601–606. https://doi.org/10.1134/S1075701513070039.

Balaram V., 2019. Rare earth elements: A review of applications, occurrence, exploration, analysis, recycling, and environmental impact. *Geoscience Frontiers*, 10(4), 1285–1303. https://doi.org/10.1016/j.gsf.2018.12.005.

Berg G., 1913. Die Erzlagerstätten der nördlichen Sudeten. *Zeitschr, zum XII Allgemeinen Deutschen Bergmannstage in Breslau. Beiträge zur Geologie Ostdeutschlands*, Breslau.

Borkowska M., 1966. Petrografia granitu Karkonoszy. *Geologica Sudetica*, 2(1), 7–119.

Cabella R., Lucchetti G. & Marescotti P., 1999. Occurrence of LREE- and Y-arsenates from a Fe-Mn deposit, Ligurian Briançonnais Domain, Maritime Alps, Italy. *The Canadian Mineralogist*, 37(4), 961–972.

Chaloupský J., 1965. Metamorphic development of the Krkonoše crystalline complex. *Krystalinikum*, 3, 31–54.

Chaloupský J., Červenka J., Jetel J., Králik F., Libalová, J., Píchová E., Pokorný J., Pošmourný K., Sekyra J., Shrbený O., Šalanský K., Šrámek J. & Václ J., 1989. *Geologie Krkonoš a Jizerských hor* [Geology of the Krkonoše and Jizera Mountains]. Ústředni Ústav Geologický, Praha.

Duthou J.L., Couturie J.P., Mierzejewski M.P. & Pin C., 1991. Oznaczenia wieku granitu Karkonoszy metodą izochronową, rubinowo-strontową na podstawie całych próbek skalnych [Next dating of granite sample from the Karkonosze Mountains using Rb-Sr total rock isochrone method]. *Przegląd Geologiczny*, 39(2), 75–78.

Förster H.J., Ondrejka M. & Uher P., 2011. Mineralogical responses to subsolidus alteration of granitic rocks by oxidizing As-bearing fluids: REE arsenates and As-rich silicates from the Zinnwald granite, eastern Erzgebirge, Germany. *The Canadian Mineralogist*, 49(4), 913–930. https://doi.org/10.3749/canmin.49.4.913.

Feigelson R.S., 1967. Crystal growth of rare-earth orthoarsenates. *Journal of the American Ceramic Society*, 50(8), 483–486. https://doi.org/10.1111/j.1151-2916.1967.tb15150.x.

Gołębiowska B., Pieczka A. & Franus W., 2006. Olivenite-adamite solid solution from oxidation zone in Rędziny (West Sudetes, Poland). *Mineralogia Polonica*, 37(2), 97–107. https://doi.org/10.2478/v10002-007-0001-1.

Gołębiowska B., Pieczka A. & Parafiniuk J., 2012. Substitution of Bi for Sb and As in minerals of the tetrahedrite series from Rędziny, Lower Silesia, southwestern Poland. *The Canadian Mineralogist*, 50(2), 267–279. https://doi.org/10.3749/canmin.50.2.267.

Gołębiowska B., Włodek A., Pieczka A., Borkiewicz O. & Polak M., 2016. The philipsbornite-segnitite solid-solution series from Rędziny, eastern metamorphic cover of the Karkonosze granite (SW Poland). *Annales Societatis Geologorum Poloniae*, 86(1), 73–83. https://doi.org/10.14241/asgp.2015.036.

Gorelikova N.V, Semenyak B.I., Korostelev P.G., Taskaev V.I., Balashov F.V. & Rassulov V.A., 2022. Rare earth minerals in the rare-metal greisens of the Verkhnee Deposit in the Khingan-Olonoisky District of the Amur Region, Russia. *Russian Journal of Pacific Geology*, 16(6), 608–623. https://doi.org/10.1134/S1819714022060033.

Graeser S. & Schwander H., 1987. Gasparite-(Ce) and monazite-(Nd): Two new minerals to the monazite group from the Alps. *Schweizerische Mineralogische und Petrographische Mitteilungen*, 67, 103–113.

Graeser S., Schwander H. & Stalder H.A., 1973. A solid solution series between xenotime ($YtPO_4$) and chernovite ($YtAsO_4$). *Mineralogical Magazine*, 39(302), 145–151. https://doi.org/10.1180/MINMAG.1973.039.302.02.

HussariX, n.d. https://github.com/sem-geologist/HussariX.

Kasatkin A.V., Stepanow S.Yu., Tsyganko M.V., Škoda R., Nestol F., Plášil J., Makovicky E., Agakhanov A.A. & Palamarchuk R.S., 2022. Mineralogy of the Vorontsovskoe gold deposit (Northern Urals). *Mineralogy*, 8(1), 5–93. http://doi.org/10.35597/2313-545X-2022-8-1-1.

Kolitsch U. & Holtstam D., 2004a. Crystal chemistry of REEXO4 compounds (X = P, As, V). I. Paragenesis and crystal structure of phosphatian gasparite-(Ce) from the Kesebol Mn-Fe-Cu deposit, Västra Götaland, Sweden. *European Journal of Mineralogy*, 16(1), 111–116. https://doi.org/10.1127/0935-1221/2004/0016-0111.

Kolitsch U. & Holtstam D., 2004b. Crystal chemistry of REEXO4 compounds (X = P, As, V). II. Review of REEXO4 compounds and their stability fields. *European Journal of Mineralogy*, 16(1), 117–126. https://doi.org/10.1127/0935-1221/2004/0016-0117.

Kozłowski A. & Sachanbiński M., 2007. Karkonosze intragranitic pegmatites and their minerals. [in:] Kozłowski A. & Wiszniewska J. (eds.), *Granitoids in Poland*, Archivum Mineralogiae Monograph, 1, Faculty of Geology of the Warsaw University, Warszawa, 155–178.

Kröner A., Hegne, E., Hammer J., Haase G., Bielicki K.H., Krauss M. & Eidam J., 1994. Geochronology and Nd-Sr systematics of Lusatian granitoids – significance for the evolution of the Variscan orogen in East-Central Europe. *Geologische Rundschau*, 83(2), 357–376. https://doi.org/10.1007/BF00210551.

Kryza R. & Mazur S., 1995. Contrasting metamorphic paths in the SE part of the Karkonosze-Izera block (Western Sudetes, SW Poland). *Neues Jahrbuch für Mineralogie*, Abhandlungen, 169, 157–192.

Kryza R., Schaltegger U., Oberc-Dziedzic T., Pin C. & Ovtcharova M., 2014. Geochronology of a composite granitoid pluton: A high-precision ID-TIMS U-Pb zircon study of the Variscan Karkonosze Granite (SW Poland). *International Journal of Earth Sciences*, 103(3), 683–696. https://doi.org/10.1007/s00531-013-0995-00.

Kusiak M.A., Dunkley D.J., Słaby E., Martin H. & Budzyń B., 2009. Sensitive high-resolution ion microprobe analysis of zircon reequilibrated by late magmatic fluids in a hybridized pluton. *Geology*, 37(12), 1063–1066. https://doi.org/10.1130/G30048A.1

Kusiak M.A., Williams I.S., Dunkley D.J., Konečny P., Słaby E. & Martin H., 2014. Monazite to the rescue: U-Th-Pb dating of the intrusive history of the composite Karkonosze pluton, Bohemian Massif. *Chemical Geology*, 364, 76–92. https://doi.org/10.1016/j.chemgeo.2013.11.016.

Li M.Y.H., Zhou M.F. & Williams-Jones A.E., 2019. The genesis of regolith-hosted heavy rare earth element deposits: Insights from the world-class Zudong deposit in Jiangxi Province, South China. *Economic Geology*, 114(3), 541–568. https://doi.org/10.5382/econgeo.4642.

Machowiak K. & Armstrong R., 2007. SHRIMP U-Pb zircon age from the Karkonosze granite. *Mineralogia Polonica – Special Papers*, 31, 193–196.

Mazur S., 1995. Strukturalna i metamorficzna ewolucja wschodniej okrywy granitu Karkonoszy w południowej części Rudaw Janowickich i Grzbiecie Lasockim [Structural and metamorphic evolution of the country rocks at the eastern contact of the Karkonosze granite in the southern Rudawy Janowickie Mts and Lasocki Range]. *Geologia Sudetica*, 29(1), 31–103.

Merlet C., 1994. An accurate computer correction program for quantitative electron probe microanalysis. *Microchimica Acta*, 114/115, 363–376. https://doi.org/10.1007/BF01244563.

Migdisov A., Guo X., Nisbet H., Xu H. & Williams-Jones A.E., 2019. Fractionation of REE, U, and Th in natural ore-forming hydrothermal systems: Thermodynamic modelling. *The Journal of Chemical Thermodynamics*, 128, 305–319. https://doi.org/10.1016/j.jct.2018.08.032.

Mikulski S., 2007. Metal ore potential of the parent magma of granite – the Karkonosze massif example. [in:] Kozłowski A. & Wiszniewska J. (eds.), *Granitoids in Poland*, Archivum Mineralogiae Monograph, 1, Faculty of Geology of the Warsaw University, Warszawa, 123–145.

Mil K., Gołębiowska B., Pieczka A. & Włodek A., 2024. Titanite from the NYF-type pegmatites of Szklarska Poręba Huta quarry, Karkonosze granite massif, SW Poland. *Acta Geologica Polonica*, 74(3), 20. https://doi.org/10.24425/agp.2024.151750.

Mochnacka K., Oberc-Dziedzic T., Mayer W. & Pieczka A., 2015. Ore mineralization related to geological evolution of the Karkonosze-Izera Massif (the Sudetes, Poland) – towards a model. *Ore Geology Reviews*, 64, 215–238. https://doi.org/10.1016/j.oregeorev.2014.07.00.1.

Ni Y., Hughes J.M. & Mariano A.N., 1995. Crystal chemistry of the monazite and xenotime structures. *American Mineralogist*, 80(1–2), 21–26. https://doi.org/10.2138/am-1995-1-203.

Oberc J., 1965. Stanowisko tektoniczne granitu Karkonoszy [The tectonic position of the Karkonosze granite]. *Biuletyn Instytutu Geologicznego*, 191, 69–109.

Oberc-Dziedzic T., Kryza R., Pin C., Mochnacka K. & Larionov A., 2009. The orthogneiss and schist complex of the Karkonosze-Izera Massif (Sudetes, SW Poland): U-Pb SHRIMP zircon ages, Nd-isotope systematics and protoliths. *Geologica Sudetica*, 41, 3–24.

Oberc-Dziedzic T., Kryza R., Mochnacka K., & Larionov, A., 2010. Ordovician passive continental margin magmatism in the Central-European Variscides. U-Pb zircon data from the SE part of the Karkonosze-Izera Massif, Sudetes, SW Poland. *International Journal of Earth Sciences*, 99(1), 27–46. https://doi.org/10.1016/j.oregeorev.2014.07.001.

Oliver G.J.H., Corfu F., & Krough T.E., 1993. U-Pb ages from SW Poland: Evidence for a Caledonian suture zone between Baltica and Gondwana. *Journal of the Geological Society of London*, 150, 355–369. https://doi.org/10.1144/gsjgs.150.2.0355.

Ondrejka M., Uher P., Pršek J. & Ozdín D., 2007. Arsenian monazite-(Ce) and xenotime-(Y), REE arsenates and carbonates from the Tisovec-Rejkovo rhyolite, Western Carpathians, Slovakia: Composition and substitutions in the (REE,Y)XO_4 system (X = P, As, Si, Nb, S). *Lithos*, 95(1–2), 116–129. https://doi.org/10.1016/j.lithos.2006.07.019.

Ondrejka M., Bačík P., Majzlan J., Uher, P., Ferenc Š., Mikuš T., Števko M., Čaplovičová M., Milovská S., Molnárová A., Rößler C. & Matthes C., 2024. Xenotime-(Gd), a new Gd-dominant mineral of the xenotime group from the Zimná Voda REE-U-Au quartz vein, Prakovce, Western Carpathians, Slovakia. *Mineralogical Magazine*, 88(5), 613–622. https://doi.org/10.1180/mgm.2024.62.

Pagliaro F., Lotti P., Guastoni A., Rotiroti N., Battiston T. & Gatta G., 2022. Crystal chemistry and miscibility of chernovite-(Y), xenotime-(Y), gasparite-(Ce) and monazite-(Ce) from Mt. Cervandone, Western Alps. *Italy Mineralogical Magazine*, 86(1), 150–167. https://doi.org/10.1180/mgm.2022.5.

Pagliaro F., Comboni D., Battiston T., Krüger H., Hejny C., Kahlenberg V., Gigli L., Glazyrin K., Liermann H.-P., Garbarino G., Gatta G.D. & Lotti P., 2024. Comparative thermal and compressional behaviour of natural xenotime-(Y), chernovite-(Y) and monazite-(Ce). *Mineralogical Magazine*, 88(6), 682–697. https://doi.org/10.1180/mgm.2024.70.

Parafiniuk J., 2003. Secondary bismuth and tellurium minerals from Rędziny (Rudawy Janowickie, SW Poland). *Mineralogia Polonica*, 34(2), 3–14.

Parafiniuk J. & Domańska J., 2002. Bismuth minerals from Rędziny (Rudawy Janowickie, SW Poland). *Mineralogia Polonica*, 33(2), 3–14.

Parafiniuk J., Pieczka A. & Gołębiowska B., 2008. Compositional data for ikunolite from Rędziny, Rudawy Janowickie, Lower Silesia, Poland. *The Canadian Mineralogist*, 46(5), 1305–1315. https://doi.org/10.3749/canmin.46.5.1305.

Pieczka A., Gołębiowska B. & Parafiniuk J., 2009. Conditions of formation of polymetallic mineralization in the eastern envelope of the Karkonosze granite: The case of Rędziny, southwestern Poland. *The Canadian Mineralogist*, 47(4), 765–786. https://doi.org/10.3749/canmin.47.4.765

Pieczka A., Gołębiowska B. & Parafiniuk J., 2011. Gold in sulfide-telluride assemblages at Rędziny, Rudawy Janowickie Range. [in:] Kozłowski A. & Mikulski S.Z. (eds.), *Gold in Poland*, Archivum Mineralogiae Monograph, 2, Faculty of Geology of the Warsaw University, Warszawa, 119–134.

Siuda R. & Gołębiowska B., 2011. Nowe dane o minerałach wietrzeniowych złoża Miedzianka-Ciechanowice w Rudawach Janowickich (Dolny Śląsk, Polska) [New data on supergene minerals from Miedzianka-Ciechanowice deposit in the Rudawy Janowickie Mountains (Lower Silesia, Poland)]. *Przegląd Geologiczny*, 59(3), 226–234.

Słaby E. & Martin H., 2008. Mafic and felsic magma interaction in granites: The Hercynian Karkonosze Pluton (Sudetes, Bohemian Massif). *Journal of Petrology*, 49(2), 353–391. https://doi.org/10.1093/petrology/egm085.

Syczewski M.D., Siuda R., Rohovec J., Matoušková Š. & Parafiniuk J., 2022. Uranyl minerals from abandoned Podgórze mine (Sudetes Mountains, SW Poland) and their REE content. *Minerals*, 12(3), 307. https://doi.org/10.3390/min12030307.

Teisseyre J.H., 1971. O wieku i następstwie warstw w skałach metamorficznych Rudaw Janowickich i Grzbietu Lasockiego [On the age and sequence of beds in the metamorphic rocks of the Rudawy Janowickie range and Lasocki Ridge]. *Geologia Sudetica*, 5(1), 165–210.

Teisseyre J., 1973. Skały metamorficzne Rudaw Janowickich i Grzbietu Lasockiego [Metamorphic rocks of the Rudawy Janowickie and Lasocki Range]. *Geologia Sudetica*, 8(1), 7–120.

Vereshchagin O.S., Britvin S.N., Perova E.N., Brusnitsyn A.I., Polekhovsky Y.S., Shilovskikh V.V., Bocharov V.N., van der Burgt A., Cuchet S. & Meisser N., 2019. Gasparite-(La), $La(AsO_4)$, a new mineral from Mn ores of the Ushkatyn-III deposit, Central Kazakhstan, and metamorphic rocks of the Wanni glacier, Switzerland. *American Mineralogist*, 104(10), 1469–1480. https://doi.org/10.2138/am-2019-7028.

Warr L.N., 2021. IMA-CNMNC approved mineral symbols. *Mineralogical Magazine*, 85(3), 291–320. https://doi.org/10.1180/mgm.2021.43

Wołkowicz K. & Wołkowicz S., 1985. Mineralizacja kruszcowa wschodniej strefy kontaktowej granitu karkonoskiego na obszarze Mniszkowa – Rędzin [Ore mineralization at eastern contact zone of the Karkonosze granite in the Mniszków – Rędziny area]. *Kwartalnik Geologiczny*, 29(2), 237–254.

Zimnoch E., 1978. Mineralizacja kruszcowa złoża Miedzianka w Sudetach. *Biuletyn Państwowego Instytutu Geologicznego*, 308(1), 91–134.